International Journal of Impact Engineering 37 (2010) 467–474

Contents lists available at ScienceDirect

International Journal of Impact Engineering

journal homepage: www.elsevier.com/locate/ijimpeng

Dynamic crushing strength of hexagonal honeycombs

L.L. Hu [a,*], T.X. Yu [b]

[a] Department of Applied Mechanics & Engineering, School of Engineering, Sun Yat-sen University, Guangzhou 510275, PR China
[b] Department of Mechanical Engineering, The Hong Kong University of Science and Technology, Clear Water Bay, Kowloon, Hong Kong

ARTICLE INFO

Article history:
Received 24 June 2009
Received in revised form
2 December 2009
Accepted 5 December 2009
Available online 16 December 2009

Keywords:
Honeycomb
Dynamic
Crushing strength

ABSTRACT

Based on the repeatable collapsing mechanism of cells' structure under dynamic crushing, an analytical formula of the dynamic crushing strength of regular hexagonal honeycombs is derived in terms of impact velocity and cell walls' thickness ratio. It is consistent with the equation obtained from the shock wave theory that regards cellular material as continuum, in which the key parameter is approximately measured from the "stress–strain" curve of the cellular material. The effect of unequal thickness of cell walls on the honeycomb's dynamic crushing strength is discussed, and the result shows that the dynamic crushing strength of the hexagonal honeycomb with some double-thickness walls is about 1.3 times of that of the hexagonal honeycomb without double-thickness wall. All of the analytical predictions are compared with the numerical simulation results, showing good agreements.

1. Introduction

As a classical species of cellular materials, honeycombs have attracted a great deal of attention owing to their outstanding properties in efficient energy absorption, high relative stiffness and strength, heat insulation, and so on. They have been widely used in lightweight structures and in energy absorption devices, especially under impact loading conditions [1]. Extensive analytical [1–4], experimental [5–7], and numerical works [5,8] have been carried out to study their mechanical properties under quasi-static compression, such as the stiffness, yield strength and buckling strength. When used in energy absorption devices, honeycombs often suffer from impact forces, so the dynamic behavior associated with the deformation mechanisms, the crushing strength and the energy absorption needs to be studied in depth.

The out-of-plane dynamic behavior of a honeycomb has attracted much attention since the honeycomb is more effective in energy absorption under out-of-plane impact than under in-plane impact. However, in some applications, such as using a honeycomb block as an energy absorption layer in aircraft against bird or debris collision, the crushing could take place along any direction of the honeycomb. Hence, the in-plane dynamic behavior of a honeycomb also needs to be known besides its out-of-plane behavior.

Localization is a characteristic feature of honeycombs under in-plane compression. In quasi-static compression, collapse first takes place at the weakest row or band of cells, which is dominated by the distribution and extent of the initial imperfections and gradually spreads to stronger areas of the structure [5,6]. The response to dynamic loadings is very different from the quasi-static one, as the structural and inertial effects will significantly influence the crushing behaviors. Localization bands would initiate at the impact end or the fixed end of the honeycomb once the impact velocity exceeds a critical value, despite initial imperfections distributed among the honeycomb [9]. Three different patterns of localization bands in uniaxially impacted honeycombs were identified based on numerical simulations [10,11]: "X" pattern, "V" pattern and "I" pattern, as shown in Fig. 1. The critical velocities, at which the pattern of localization bands changed, were studied empirically based on massive numerical results [10–12] and theoretically using thermodynamics arguments [13]. The "X" pattern usually takes place under lower impact velocity (typically on the order of 1 m/s), which is called "quasi-static localization mode" in the present paper, while the "I" pattern takes place under higher impact velocity (typically on the order of 100 m/s), which is called "dynamic localization mode" in the present paper; the "V" pattern is a transitional mode between these.

So far the majority of research interests have been mainly focused on the crushing strength of the honeycomb, as it is important for energy absorption. When the impact velocity is sufficiently high, the localization band will develop in the "dynamic localization mode" (i.e. form an "I" pattern) and propagate layer by layer from the impact end to the fixed end. This progressive densification can be regarded as a "structural shock" in cellular materials, which is similar to the propagation of a shock wave in

* Corresponding author.
E-mail addresses: llhu_80@163.com, hulingl@mail.sysu.edu.cn (L.L. Hu).

0734-743X/$ – see front matter © 2009 Elsevier Ltd. All rights reserved.
doi:10.1016/j.ijimpeng.2009.12.001

continuum. Hence, by treating a cellular material as continuum represented by a rigid–perfectly plastic–locking material model, and employing the one-dimensional shock wave theory, the dynamic crushing strength of cellular material was derived in terms of impact velocity as [14]:

$$\sigma_d = \sigma_0 + \frac{\rho^*}{\varepsilon_d} V^2 = \sigma_0 + AV^2 \quad (1)$$

where σ_d and σ_0 denote the crushing strengths of the cellular material under dynamic crushing and under quasi-static compression, respectively; ρ^* is the initial density of the cellular material, which for honeycombs is a function of the ratio between the cell wall thickness h and the cell wall length l; ε_d is the locking strain (i.e., the densification strain) under quasi-static compression, which is obtained from the "stress–strain" curve of the cellular material under quasi-static uniaxial compression; V is the impact velocity; and $A = \rho^*/\varepsilon_d$ is a material parameter. Since ρ^* and ε_d both vary with the cell walls' thickness ratio h/l, A should be a function of h/l, too. For hexagonal honeycombs, based on finite element simulations under high velocities impact, Ruan et al. [10] formulated an empirical equation to determine parameter A in terms of h/l; they then derived an empirical formula for dynamic crushing strength in terms of thickness ratio h/l and impact velocity V.

In the present paper, we deduce an analytical formula for the dynamic crushing strength in terms of the impact velocity and the thickness ratio for hexagonal honeycombs based on the collapse mechanism of cell structures under impact conditions. As a result, the locking strain of the honeycomb will be related to the honeycomb's relative density. Finally, the effect of unequal thickness of cell walls on the honeycomb's dynamic crushing strength will be discussed.

2. Numerical analysis

To understand the dynamic deformation behaviors of the hexagonal honeycomb, a finite element model is built using ANSYS-LSDYNA, as shown in Fig. 2. The hexagonal honeycomb block consists of 21 cells in the x_1 direction and 13 cells in the x_2 direction. It is placed on a fixed rigid base at one end and crushed along the x_1 direction by a rigid plate with a constant impact velocity V at the other end. The edge length of the cells is $l = 4$ mm, and the cell walls' thickness is $h = 0.346$ mm, which corresponds to a relative density of the honeycomb $\frac{\rho^*}{\rho_s} = \frac{2}{\sqrt{3}}\frac{h}{l} = 0.1$, where ρ_s is the density of the base material. The out-of-plane thickness of the honeycomb is $b = 0.5$ mm. The cell wall material is assumed to be elastic, perfectly plastic with $E = 68$ GPa, $\sigma_{ys} = 130$ MPa, $\rho_s = 2700$ kg/m^3 and $\nu = 0.3$, where E, σ_{ys}, ρ_s and ν are the Young's modulus, yield stress, density and Poisson ratio, respectively, of the base material. The material of the rigid plates is chosen to be mild steel with

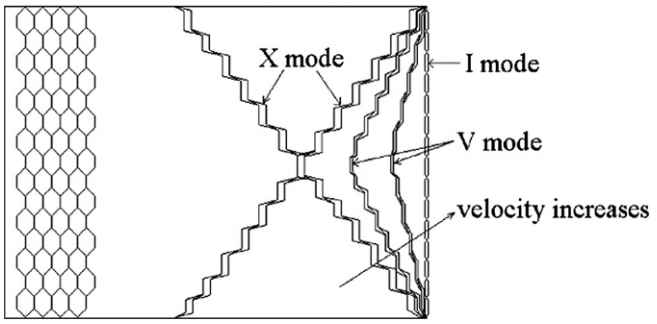

Fig. 1. Sketch of the three types of deformation modes in uniaxially impacted honeycombs [10].

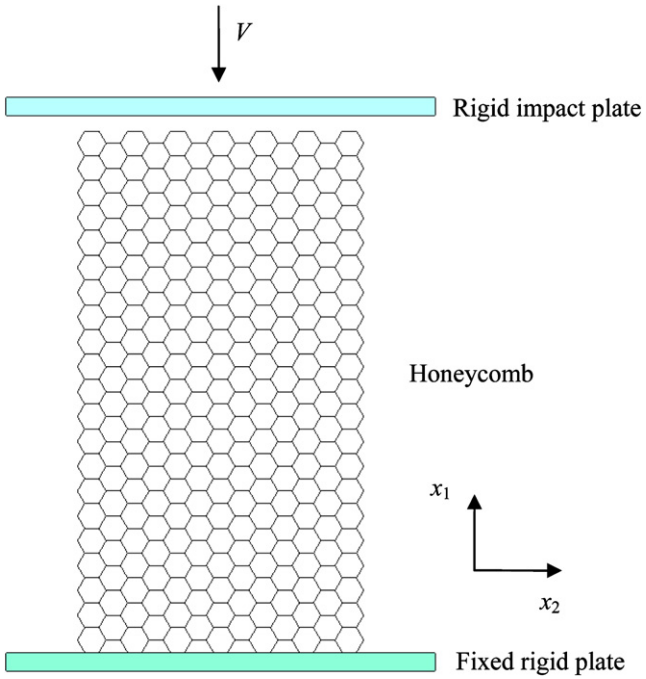

Fig. 2. FE model in the simulation.

Young's modulus 210 GPa and density 7800 kg/m^3. Each cell wall is meshed into 16 shell elements with one-layer elements along the out-of-plane direction (i.e., the x_3 direction). The out-of-plane displacement of the nodes within the x_1–x_2 plane (i.e., $x_3 = 0$) is constrained so as to prevent the specimen from out-of-plane bulking. A single self-contact is defined on the honeycomb model, and a surface-to-surface contact is applied between the honeycomb specimen and the two rigid plates respectively without considering contact friction.

A snap-shot of the deformed configuration of the honeycomb block during the crushing process under impact velocity 100 m/s is depicted in Fig. 3. The localization band initiates at the loading end perpendicular to the impact direction, and continues to propagate layer by layer to the fixed end, which exhibits the "dynamic localization mode" of honeycombs as previously reported by Ruan et al. [10] and Zou et al. [11].

By zooming in the cells' collapse process during the propagation of the localization band, as shown in Fig. 4, it is found that the cells collapse to densification layer by layer in a progressive and repeatable process. The densified cells are closely packed in a ripple form and move down together with the striker, resulting in a "zigzag" collapse front of the cells on the layer next to the densified region, while the cells on the other layers remain almost intact.

The repeatable collapse process of a typical cluster of cells, as marked within the rectangles surrounded with continuous lines shown in Fig. 4, is focused on and exhibited in Fig. 5. At the beginning of the collapse period, as shown in Fig. 5a, all of the cell walls not jointing the densified region, except for wall CD, almost remain at their original positions as sides of regular hexagons. During the whole collapse process, points A and D move downward, while points F, G and H almost hold still. At the initial state of the cells' collapse process, cell walls BF and CG rotate around points F and G respectively until AB contacts with the densified region, as shown in Fig. 5b. Then BF gradually forms a curve from a straight line and CG still rotates around point G until walls CD and BC orderly become the new front of the densified region, see Fig. 5c

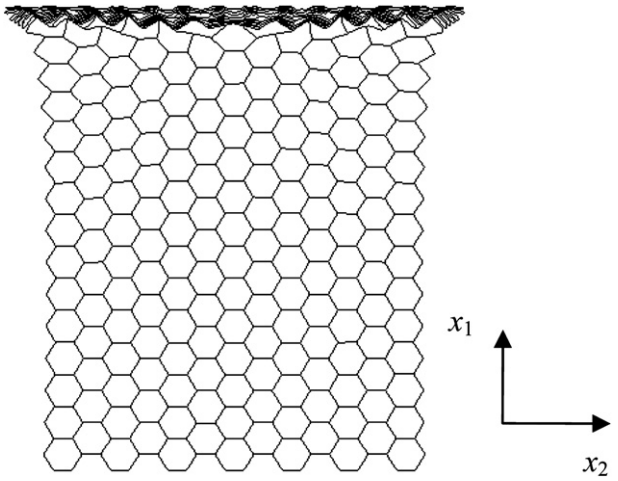

Fig. 3. Dynamic localization mode of a honeycomb.

and d. Thus, a period of the cells' collapse process is completed, and thereafter a new period will start immediately. A representative block for the new collapse period is marked by a rectangle surrounded with dashed lines in Fig. 4c, which is the same as the beginning state of the block for the old period as marked in Fig. 4a and shown in Fig. 5a.

Because of the repeatable and periodical process of the cells' collapse, the final state of a collapse period is identical to the initial state of the next period, implying certain geometric and kinematic conditions between the initial state and the final state of a collapse period, as elaborated in the following sections.

3. Dynamic crushing strength

3.1. A representative block and its deformation process

In view of the periodic characteristics of hexagonal honeycombs both in the geometric structure and in the cells' collapse process, a representative block within the honeycomb across three hexagonal cells with nine cell walls is employed, as shown in Fig. 6a. The representative block possesses original width $L_0 = 3l$ and original height $H_0 = \frac{3\sqrt{3}l}{2}$. It is noted that the whole honeycomb block can be produced by periodically placing this representative block along both the x_1 and the x_2 directions.

During a period of the repeatable collapse process of the cells associated with the propagation of the dynamic localization band, the initial ($t = t_0$) and the final ($t = t_f$) configurations of the representative block are shown in Fig. 6b and c, respectively, which correspond to the deformation configurations of cells in the FE simulation shown in Fig. 5a and d, respectively. Here t denotes the time; t_0 and t_f are the time instant at the initiation and at the end of a collapse period, respectively. σ_1 and σ_2 are the crushing stress applied on the top of the representative block and the supporting stress applied from its bottom, respectively. Since the densified region of the honeycomb moves at a constant velocity V, σ_1 is equal to the contact stress between the striker and the honeycomb block, which is exactly the crushing strength of the honeycomb that we are interested in. σ_2 is equal to the supporting stress on the honeycomb provided by the fixed end because the uncollapsed cells beyond the representative block are almost in static equilibrium.

The chain lines in Fig. 6b, such as AK, KL and LD, represent the ripple front of the densified region, within which the cell walls are packed closely along the ripple boundaries, and the newly collapsed cells will also be packed in this way. It is assumed that the representative block remains its width L_o during the collapse process, which is verified by the FE simulations that the honeycomb block show very little expansion along the x_2 direction even after being crushed to densification. Thus, by equating L_o to the projection of the boundary ripples within the representative block in the x_2 direction, the angles between the ripple front and the x_2 direction, α, is found as

$$\alpha = \arccos\frac{3}{4} \tag{2}$$

At the beginning instant of a collapse period of the representative block, as shown in Fig. 6b, all the cell walls, excepting walls CD and DE, remain in their original positions and configurations as sides of regular hexagons without any deformation or rotation. Wall DE has just joined the densified region moving with a constant velocity V, while wall CD has deformed to a curve from a straight line. Based on the numerical simulation results, the positions of points F, G and H are assumed to remain unchanged during the whole collapse period ($t_0 \le t \le t_f$), although they will gain a velocity at the end instant of the collapse period ($t = t_f$). Thus, at the beginning of the collapse period cell walls FI, GJ and GH hold still, i.e.,

$$\vec{p}_{\mathrm{FI}} = \vec{p}_{\mathrm{GJ}} = \vec{p}_{\mathrm{GH}} = 0 \tag{3}$$

where $\vec{p}$ is the momentum of cell walls. In Fig. 6b, both points A and D have just joined the densified region, so they gain a downward constant velocity V at the beginning instant of the collapse period, resulting in non-zero momentum of cell walls AB, BC, CD, BF and CG, which is obvious from the velocity vector-graph of some points, as shown in Fig. 6b.

Fig. 6c sketches the final configuration of the representative block at the end of a collapse period, which also represents the beginning of the next period. At this moment, the final height of the representative block is $H_f = \sqrt{3}l + \frac{h}{\cos\alpha}$. Cell walls AB, BC and CD in Fig. 6b now have formed the new ripple front and become a part of the densified region, as marked as A′B′, B′C′ and C′D′ accordingly in Fig. 6c. Hence, all these walls have gained the same velocity V as

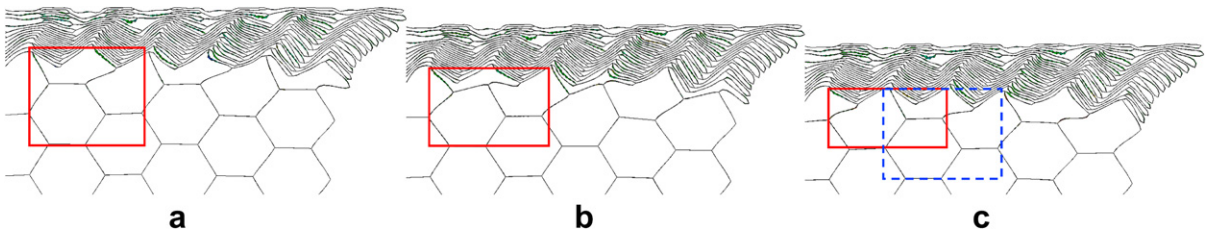

Fig. 4. A repeatable collapse process of the cells during the propagation of dynamic localization band: (a) at the beginning, (b) in the course, and (c) at the end.

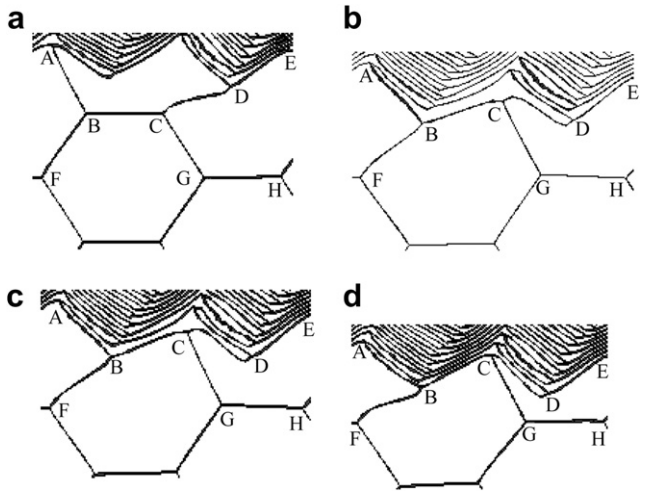

Fig. 5. A typical period of the repeatable collapse process of cells in the FE simulation.

that of the striker. The curving edge CD shown in Fig. 6b has now become straight line C′D′ at the end of the collapse period, see Fig. 6c, while FB becomes curved line F′B′, which is the same as the initial state of CD shown in Fig. 6b. The state of wall C′G′ in Fig. 6c is the same as that of AB in Fig. 6b because of the periodicity in both the geometry and the collapse process of the honeycomb; and the same states also exist between F′I′ and CG, G′H′ and BC, and between G′J′ and BF. Besides, it is noted that cell wall DE remains at the boundary of the densified region during the whole collapse period. Considering all these kinematic conditions, the following relationships should be held:

$$\begin{aligned}&\overrightarrow{p}_{F'B'} = \overrightarrow{p}_{CD};\ \overrightarrow{p}_{C'G'} = \overrightarrow{p}_{AB};\ \overrightarrow{p}_{D'E'} = \overrightarrow{p}_{DE};\\ &\overrightarrow{p}_{F'I'} = \overrightarrow{p}_{CG};\ \overrightarrow{p}_{G'H'} = \overrightarrow{p}_{BC};\ \overrightarrow{p}_{G'J'} = \overrightarrow{p}_{BF}\end{aligned} \tag{4}$$

3.2. Dynamic crushing strength

Consider a complete collapse period of the representative block from $t = t_0$ (Fig. 6b) to $t = t_f$ (Fig. 6c). Based on the theorem of linear momentum, the difference between the impulses of σ_1 and σ_2 in the time interval is equal to the change of the momentum in the x_1 direction of the nine cell edges involved in the representative block, i.e.,

$$\begin{aligned}&bL_o\int_{t_o}^{t_f}(\sigma_1-\sigma_2)dt\\ &=\left(p^{x_1}_{A'B'}+p^{x_1}_{B'C'}+p^{x_1}_{C'D'}+p^{x_1}_{D'E'}+p^{x_1}_{F'B'}+p^{x_1}_{C'G'}+p^{x_1}_{F'I'}+p^{x_1}_{G'J'}+p^{x_1}_{G'H'}\right)\\ &-\left(p^{x_1}_{AB}+p^{x_1}_{BC}+p^{x_1}_{CD}+p^{x_1}_{DE}+p^{x_1}_{FB}+p^{x_1}_{CG}+p^{x_1}_{FI}+p^{x_1}_{GJ}+p^{x_1}_{GH}\right)\end{aligned} \tag{5}$$

where p^{x_1} denotes the momentum along the x_1 direction of the cell wall. By using Eqs. (3) and (4), Eq. (5) is simplified as

$$bL_o\int_{t_o}^{t_f}(\sigma_1-\sigma_2)dt = p^{x_1}_{A'B'}+p^{x_1}_{B'C'}+p^{x_1}_{C'D'} \tag{6}$$

The velocity of cell walls A′B′, B′C′ and C′D′ in Fig. 6c is equal to the striker's velocity V, thus,

$$p^{x_1}_{A'B'} = p^{x_1}_{B'C'} = p^{x_1}_{C'D'} = \rho_s hblV \tag{7}$$

Hence, with $L_o = 3l$ for regular hexagonal honeycombs, Eq. (6) leads to

$$\int_{t_o}^{t_f}\sigma_1 dt = \rho_s hV + \int_{t_o}^{t_f}\sigma_2 dt \tag{8}$$

Since no collapse takes place in the cells between the collapsing band and the supporting rigid plate, the value of σ_2 should not larger than the cells' quasi-static collapse strength σ_0, i.e., σ_0 should be a upper limit of σ_2. Here we further assume that σ_2 keeps a constant at its limit value, σ_0, over the entire collapse period; and the error caused by this assumption can be ignored, as will be verified below, in estimating the crushing strength of honeycombs under dynamic conditions.

Thus, by noting $\sigma_0 = \frac{2}{3}\sigma_{ys}(\frac{h}{l})^2$ (refer to Ref. [1]) and $t_f - t_o = (\frac{\sqrt{3}l}{2} - \frac{h}{\cos\alpha})/V$, the average crushing strength of the honeycomb over a collapse period, σ_d, is expressed as

$$\sigma_d = \frac{1}{t_f - t_o}\int_{t_o}^{t_f}\sigma_1 dt = \frac{2}{3}\sigma_{ys}\left(\frac{h}{l}\right)^2 + \frac{6\left(\frac{h}{l}\right)\rho_s}{3\sqrt{3}-8\left(\frac{h}{l}\right)}V^2 \tag{9}$$

which provides an analytical expression of the dynamic crushing strength of regular hexagonal honeycombs in terms of the impact velocity and the thickness ratio of cells. It indicates that the dynamic crushing strength of honeycombs increases with the impact velocity by a square law, which is in agreement with the previous findings [10,14,15] obtained from various approaches. As the second term at the right-hand side of Eq. (9) is proportional to $\rho_s V^2$, it is evident that this item is resulted from the inertia effect.

Fig. 7 compares the theoretical prediction obtained from Eq. (9) and our numerical simulation result, confirming that Eq. (9) can well predict the crushing strength of the hexagonal honeycombs under dynamic crushing.

Ruan et al. [10] reported more cases which simulated the large deformation process of aluminum hexagonal honeycombs crushed in the x_1 direction with the variations in both the cell wall thickness and the impact velocity. In all those cases, the density and the yield stress of the base material were taken as 2700 kg/m^3 and 76 MPa, respectively. The crushing strengths of honeycombs in the cases with the dynamic localization mode are summarized in Table 1 to compare with the theoretical predictions obtained from Eq. (9). The comparison is also depicted in Fig. 8. Both Table 1 and Fig. 8 indicate that the theoretical expression Eq. (9) results in a good agreement with the numerical simulation data. The deviations of the former from the latter are no more than 7.15%.

In the above, the supporting stress σ_2 is assumed to be constant and equal to its upper limit value σ_0, which is the cells' quasi-static collapse strength, over the entire crushing process. σ_0 is included in the expression of σ_d as the first item on the right hand side of Eq. (9). Table 1 lists the values of σ_0 and the ratios of σ_0 to σ_d for all the cases involved. It is shown that the proportion of σ_0 in σ_d is no more than 10%, except for two cases. That is to say, the first item in the right hand of Eq. (9) has little influence on σ_d. So the error from this item caused by assuming σ_2 to be equal to its upper limit value σ_0 is negligible for predicating the dynamic crushing strength σ_d. For the two cases of $h/l = 0.074$, $V = 70$ m/s and $h/l = 0.111$, $V = 100$ m/s, the ratios between σ_0 and σ_d are larger than 10%, whereas they are the transitional cases, in which the localization bands of crushed honeycombs transform from "V" pattern to "I" pattern [10]. Consequently, the supporting stress of the respective block σ_2 in these two cases is very close to σ_0, as several layers of cells deform simultaneity in the "V" pattern cases [10]. In fact, by tracking the

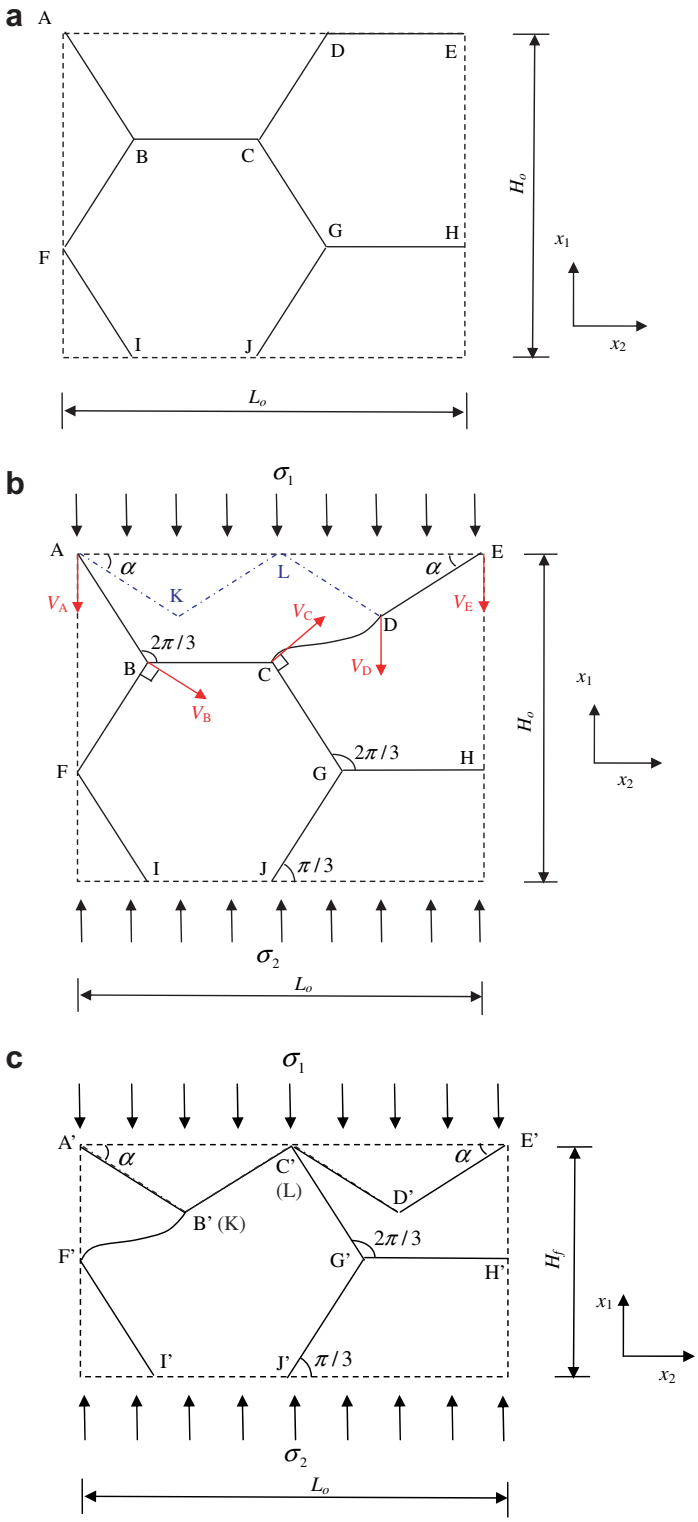

Fig. 6. (a) A representative block; (b) the initial configuration of the representative block at the beginning of a period of collapse process ($t = t_0$); and (c) the final configuration of the representative block at the end of a period of collapse process ($t = t_f$).

supporting stress on the honeycomb provided by the fixed end during the crushing process, it is found that the supporting stress, σ_2, oscillates around the quasi-static crushing strength, σ_0, of the honeycomb as shown in Fig. 9, which was also verified in the FE simulations by Zou et al. [11]. It provides another warranty that assuming σ_2 being equal to σ_0 is reasonable.

Eq. (9) shows that the dynamic crushing strength of a honeycomb includes two parts: one is the quasi-static crushing strength of the honeycomb, which is determined by its own attribution of the cellular material (see the first item at the right hand side of Eq. (9)); and the other one, i.e., the second item at the right-hand side of Eq. (9), is a result of the inertia effect. The ratios of σ_0 to σ_d listed

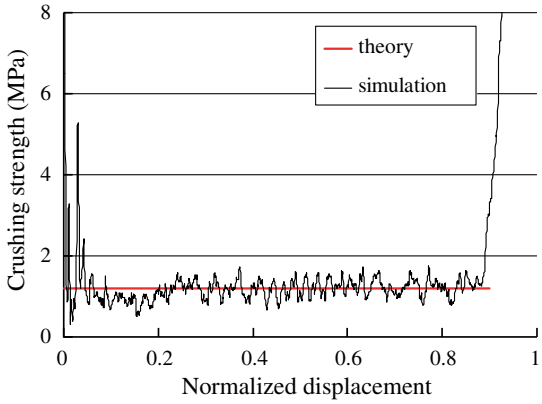

Fig. 7. Comparison of the theoretical prediction by Eq. (9) with the simulation result reported in this paper ($V = 50$ m/s).

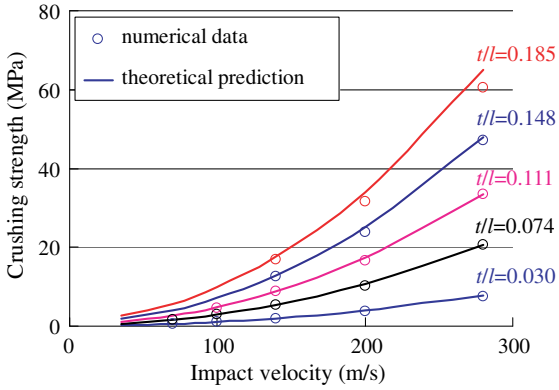

Fig. 8. Comparison of the theoretical predictions by Eq. (9) with the numerical results reported in Ref. [10].

in Table 1 show that under dynamic crushing conditions, about 90% of the crushing strength of a honeycomb is attributed by the inertia effect, while the contribution by the self attribution of the honeycomb is only about 10%. In other words, the dynamic crushing strength of a honeycomb is dominated by the inertia effect, which explains why the honeycomb possesses a much higher crushing strength under impact loading compared with that under quasi-static conditions, and this enhancement is more prominent with higher impact velocity because the inertia effect becomes much more significant.

4. Discussion

4.1. Locking strain

Based on the periodical characteristics of hexagonal honeycombs during the cells' collapse process under dynamic crushing, an analytical formula of dynamic crushing strength of hexagonal honeycombs is derived in terms of impact velocity and cell walls' thickness ratio, as given by Eq. (9). By noting that the initial density of hexagonal honeycomb is $\rho^* = \frac{2}{\sqrt{3}}\frac{h}{l}\rho_s$, Eq. (9) can be re-written as

$$\sigma_d = \frac{2}{3}\sigma_{ys}\left(\frac{h}{l}\right)^2 + \frac{\rho^*}{1-\left(\frac{1}{\cos\alpha}\right)\left(\frac{\rho^*}{\rho_s}\right)}V^2 = \frac{2}{3}\sigma_{ys}\left(\frac{h}{l}\right)^2 + \frac{\rho^*}{1-\frac{4}{3}\left(\frac{\rho^*}{\rho_s}\right)}V^2 \tag{10}$$

Recall that Eq. (1) obtained by Reid and Peng [14] was derived from the one-dimensional shock wave theory by regarding the cellular material as continuum with a rate-independent, rigid–perfectly plastic–locking material model. Under those conditions, Eq. (10) and Eq. (1) will be identical with each other when

$$\sigma_0 = \frac{2}{3}\sigma_{ys}\left(\frac{h}{l}\right)^2 \tag{11}$$

and

$$\varepsilon_d = 1 - \left(\frac{1}{\cos\alpha}\right)\frac{\rho^*}{\rho_s} = 1 - \frac{4}{3}\frac{\rho^*}{\rho_s} \tag{12}$$

It is recalled that in the theory of Reid and Peng, the locking strain ε_d is approximately obtained by constructing tangent lines on the quasi-static "stress–strain" curves of the cellular material [14]. Here Eq. (12) provides an analytical formula on the locking strain of the regular hexagonal honeycomb crushed with dynamic localization mode.

By contrasting with the expression on the densified strain of cellular material in Ref. [1], i.e.,

$$\varepsilon_d = 1 - \frac{\rho^*}{\rho_s} \tag{13}$$

Table 1
The crushing strength of honeycombs

h/l	V (m/s)	Dynamic crushing strength σ_d (MPa)			σ_0 (MPa)	σ_0/σ_d (%)
		Analytical	Numerical [10]	Deviation (%)		
0.030	70	0.52	0.56	6.70	0.04	8.57
	100	1.01	1.06	4.58	0.04	4.39
	140	1.94	1.96	0.89	0.04	2.29
	200	3.92	3.73	4.96	0.04	1.14
	280	7.63	7.55	1.15	0.04	0.58
0.074	70	1.56	1.60	2.80	0.28	17.88
	100	2.88	2.97	2.74	0.28	9.64
	140	5.39	5.38	0.17	0.28	5.16
	200	10.70	10.29	4.07	0.28	2.60
	280	20.71	20.49	1.09	0.28	1.34
0.111	100	4.80	4.68	2.73	0.63	13.02
	140	8.82	8.78	0.37	0.63	7.09
	200	17.34	16.70	3.84	0.63	3.61
	280	33.39	33.50	0.33	0.63	1.87
0.148	140	12.84	12.50	2.72	1.11	8.66
	200	25.05	23.70	5.68	1.11	4.44
	280	48.02	47.01	2.16	1.11	2.32
0.185	140	16.98	17.57	3.32	1.74	9.89
	200	31.70	34.04	6.89	1.74	5.10
	280	60.40	65.05	7.15	1.74	2.67

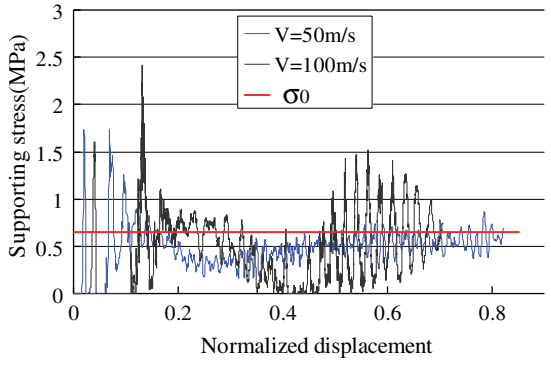

Fig. 9. Comparison of the supporting stress on a honeycomb with the quasi-static crushing strength σ_0.

Eq. (12) provides a modification to Eq. (13) with the modificatory item of $(1/\cos\alpha) = 1.33$, which reflects the packing form of the cell walls in the dynamic localization mode.

4.2. Unequal thickness

Most of the widely used metal honeycombs and Nomex honeycombs are extended from the equidistantly-glued metal foil or Nomex foil, so the thickness of the cell walls parallel to the x_2 direction is double of that unparallel to the x_2 direction, as depicted in Fig. 10. Here, we call this kind of honeycomb "double-thickness honeycomb", and the honeycomb with all of the cell walls possessing the same thickness as discussed in the above sections is called "single-thickness honeycomb". In the following, the dynamic crushing strength of the double-thickness honeycomb is analyzed following the method used in Section 3. For other kinds of unequal-thickness honeycombs, their dynamic crushing strength can be obtained similarly.

For the double-thickness honeycomb, the representative block shown in Fig. 6 and Eqs. (2)–(6) are still tenable, while Eq. (7) is substituted with

$$p^{x_1}_{A'B'} = p^{x_1}_{C'D'} = \rho_s hblV,\quad p^{x_1}_{B'C'} = 2\rho_s hblV \tag{14}$$

where h is the thickness of the cell walls unparallel to the x_2 direction; consequently the thickness of the cell walls parallel to the x_2 direction is $2h$. Thus, by submitting Eq. (14) to Eq. (6), Eq. (8) is replaced by

$$\int_{t_o}^{t_f} \sigma_1 dt = \frac{4}{3}\rho_s hV + \int_{t_o}^{t_f} \sigma_2 dt \tag{15}$$

Therefore, the average dynamic crushing strength of the double-thickness honeycomb σ_d is obtained as

$$\sigma_{\mathrm{d}} = \frac{1}{t_f - t_o}\int_{t_o}^{t_f} \sigma_1 dt = \frac{2}{3}\sigma_{\mathrm{ys}}\left(\frac{h}{l}\right)^2 + \frac{8\left(\frac{h}{l}\right)\rho_s}{3\sqrt{3} - 8\left(\frac{h}{l}\right)}V^2 \tag{16}$$

The analysis in Section 3.2 indicates that the dynamic crushing strength of a honeycomb is dominated by the inertia effect, which is represented by the second item in the right hand of Eq. (9) and Eq. (16). Thus, by comparing Eq. (16) with Eq. (9), it is obvious that the dynamic crushing strength of the double-thickness honeycomb is about 1.3 times of that of the single-thickness honeycomb, which can be further confirmed by the simulation results shown in Fig. 11. The relationship of the dynamic crushing strengths σ_d between the double-thickness honeycomb and the single-thickness honeycomb obtained by the FE simulations is exhibited in Fig. 11 under three levels of crushing velocity: 50 m/s, 100 m/s and 150 m/s, respectively. These two kinds of honeycomb possess the same material parameters and geometry parameters as described in Section 2 except for the thickness of the cell walls parallel to the x_2 direction. It is obvious from Fig. 11 that the relationship of σ_d between the two kinds of honeycomb is very close to the line of $y = 1.3x$, i.e., the dynamic crushing strength of the double-thickness honeycomb is about 1.3 times of that of the single-thickness honeycomb.

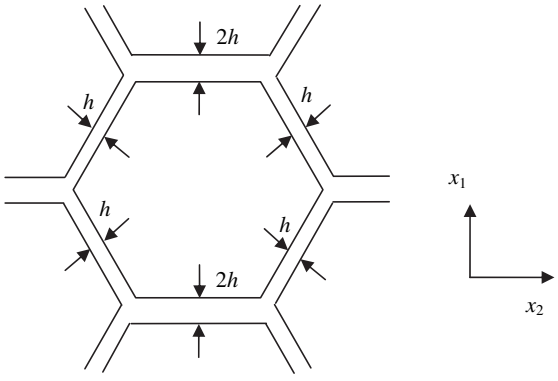

Fig. 10. Sketch of the double-thickness honeycomb.

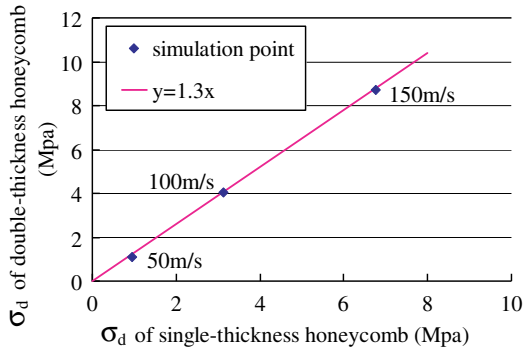

Fig. 11. Dynamic crushing strength σ_d for the double-thickness honeycomb and the single-thickness honeycomb.

5. Summary

In the present work, the dynamic behaviors of hexagonal honeycombs are analyzed from a structural point of view instead of continuum; nevertheless the result is consistent with that obtained from the theory of continuum, so that the consistency does exist between the two theories on the mechanical behaviors of cellular materials. With the structural point of view as adopted in this paper, a thorough analytical formula on the dynamic crushing strength of the honeycomb is obtained by studying the repeatable collapsing processes of the cell structure, and the prediction is in good agreements with the numerical simulation results.

As a side product of this analytical formula on the dynamic crushing strength, the locking strain of the honeycomb can be explicitly expressed by Eq. (12); while previously the locking strain, defined in the rigid–perfectly plastic–locking model, could only be approximately measured from the quasi-static "stress–strain" curve of cellular materials as proposed by Reid and Peng [14]. The expression of the locking strain also provides a modification to the Gibson–Ashby formula [1] on the densified stain of cellular material, and the modificatory item well reflects the packing form of the cell walls in the dynamic densification process.

The effect of the unequal thickness of the cell walls on the honeycomb's dynamic crushing strength is also analyzed and discussed. Both of the analytical formulas and the numerical results show that the dynamic crushing strength of the double-thickness honeycomb is about 1.3 times of that of the single-thickness honeycomb.

Acknowledgments

The authors would like to thank the support from the National Natural Science Foundation of China under grant No. 10802100 and Key Project No. 10532020.

References

[1] Gibson LJ, Ashby MF. Cellular solids: structure and properties. 2nd ed. Cambridge University Press; 1997.
[2] Karagiozova D, Yu TX. Plastic deformation modes of regular hexagonal honeycombs under in-plane biaxial compression. Int J Mech Sci 2004;46:1489–515.
[3] Karagiozova D, Yu TX. Post-collapse characteristics of ductile circular honeycombs under in-plane compression. Int J Mech Sci 2005;47:570–602.
[4] Okumura D, Ohno N, Noguchi H. Elastoplastic microscopic bifurcation and post-bifurcation behavior of periodic cellular solids. J Mech Phys Solids 2004;52:641–66.
[5] Hu LL, Yu TX, Gao ZY, Huang XQ. The inhomogeneous deformation of polycarbonate circular honeycombs under in-plane compression. Int J Mech Sci 2008;50:1224–36.
[6] Papka SD, Kyriakides S. In-plane compressive response and crushing of honeycombs. J Mech Phys Solids 1994;42:1499–532.
[7] Papka SD, Kyriakides S. Biaxial crushing of honeycombs-Part I: Experiments. Int J Solids Struct 1999;36(29):4367–96.
[8] Papka SD, Kyriakides S. Biaxial crushing of honeycombs-Part II: Analysis. Int J Solids Struct 1999;36(29):4397–423.
[9] Honig A, Strong WJ. In-plane dynamic crushing of honeycomb. Part I, crush band initiation and wave trapping. Int J Mech Sci 2002;44:1665–96.
[10] Ruan D, Lu G, Wang B, Yu TX. In-plane dynamic crushing of honeycombs—finite element study. Int J Impact Eng 2003;28:161–82.
[11] Zou Z, Reid SR, Tan PJ, Li S, Harrigan JJ. Dynamic crushing of honeycombs and features of shock fronts. Int J Impact Eng 2009;36:165–76.
[12] Zheng Z, Yu J, Li J. Dynamic crushing of 2D cellular structures: a finite element study. Int J Impact Eng 2005;32:650–64.
[13] Tan PJ, Reid SR, Harrigan JJ, Zou Z, Li S. Dynamic compressive strength properties of aluminium foams. Part II—'shock' theory and comparison with experimental data and numerical models. J Mech Phys Solids 2005;53:2206–30.
[14] Reid SR, Peng C. Dynamic uniaxial crushing of wood. Int J Impact Eng 1997;19:531–70.
[15] Lu G, Yu TX. Energy absorption of structures and materials. Cambridge, UK: Woodhead Publishing Ltd; 2003.

Nomenclature

A: a parameter, $A = \rho^*/\varepsilon_d$
b: out-of-plane thickness of honeycomb
E: Young's modulus of base material
h: cell wall thickness of honeycomb
H_o: original height of the representative block
H_f: final height of the representative block
L_o: original length of the representative block
l: cell wall length of honeycomb
$\vec{p}$: momentum
p^{x_1}: momentum along the x_1 direction
t_0: time instant at the beginning of a collapse period
t_f: time instant at the end of a collapse period
V: impact velocity
ε_d: locking strain or densified strain of cellular material under quasi-static compression
α: angle of the ripple boundaries of densified region, seen in Fig. 6b
υ: Poisson ratio of base material
ρ^*: initial density of cellular material
ρ_s: density of base material
σ_0: cells' quasi-static collapse strength, quasi-static crushing strength of cellular material
σ_d: dynamic crushing strength
σ_{ys}: yield stress of base material
σ_1: crushing stress suffered by the representative block
σ_2: supporting stress applied to the representative block